Microstructural 4D printing investigation of ultra-sonication biocomposite polymer

Oladapo, Bankole I.; Adebiyi, Aderogba V.; Ifeoluwa Elemure, E.

Published in:
Journal of King Saud University - Engineering Sciences

DOI:
10.1016/j.jksues.2019.12.002

Publication date:
2021

Journal of King Saud University – Engineering Sciences 33 (2021) 54–60

Contents lists available at ScienceDirect

Journal of King Saud University – Engineering Sciences

journal homepage: www.sciencedirect.com

Original article

Microstructural 4D printing investigation of ultra-sonication biocomposite polymer

Bankole I. Oladapo [a,*], Aderogba V. Adebiyi [a], E. Ifeoluwa Elemure [b]

[a] School of Engineering and Sustainable Development, De Montfort University, Leicester, UK
[b] Department of Mechanical and Design Engineering, University of Portsmouth, UK

ARTICLE INFO

Article history:
Received 1 July 2019
Accepted 3 December 2019
Available online 10 December 2019

Keywords:
4D printing
Ultra-sonication
Cellulose-hydrogel
Polymer composite

ABSTRACT

This research focuses on **computational** microstructure to create hydrogel-cellulose ultra-sonication method for the production of additive structures and the stability of the physical characteristics of its cellulose hydrographic composite material in 4D printing. CMC with combined cellulose fibres of high cellulose content for dispersion compounds and fine dehydrated particles allows a 50% fibre matrix hydrolysis. Evaluation of the microstructure composite particle of CMC in 4D surface luminance structure and the profile structure was done. Cross-sectional views and surface roughness, waviness profile of the specimens are extracted and analysed, with the coresonding Gaussian filter for accurate decomposition of particles was carry out. The nanoparticle characterisation of the thermoplastic form was used in the mixed sedimentation process to create an polymer composite structure when analyse. The shrinkage properties of the materials are evaluated to understand the relationship between the deformation according to the time and direction of the 4D printing analysis. The ability of **computational** ultra-sonication microstructure to be used correctly for 4D printing is demonstrated by evaluating a complex microstructure that can change with time according to the predefined design rules to respond to moisture. The most critical feature is the cellulose gratified in the ultimate material model, which is the amount of cellulose of the ultra-sonication composite specified in the 4D printing materials of 2.5% by mass of hydrogen and 2.5% by mass of CMC.

1. Introduction

The research community sought new ways to develop sensitive structures that could familiarise to variations in the situation (Bakarich and Spinks, 2015; Zhu, 2012; Bankole et al., 2018a). New chemical materials in the position Materials for the response from the moisture-absorbing pineapple transplant Heliotrope SunTracking behaviour in plants such as Sunflower and Malva and the reaction of the plants. Delicate balsam and many carnivorous plants perfect example of a structure that responds to various stimuli for efficiency. (Xin, 2017) Therefore, there are many significant research efforts and scientific literature. (Demitri, 2008) In the implementation of passive response, systems are following: (i) respond to stimuli that meet needs (ii) Methods for controlling the placement of sensitive materials objectives of the system response Precision materials, cellulose Potential of materials are price precursors, biodegradable, biodegradable and programmable (Xin, 2017; Bankole et al., 2019). The most abundant cellulose in bio-nature. Molecules connected to anhydrous-d-glucose in which each unit will return to 180 adjacent units (Håkansson and Gatenholm, 2016; Ana et al., 2018). Presence of hydroxyl group. The molecule Hydrogen bonds between atoms occur on structure (Chang 2011) binds to the crystalline phase and in an amorphous manner. The introduction of water into the cellulose can lead to amorphous compositions to reduce or loosen hydrogen bonds by the creation of hydrogen bonds in the competitive area (Zheng 2015, Bankole et al., 2018b). The complexity of the structure of the biological system behaves according to the hierarchy. Elimination of tension in the substrate is the driving force behind most changes in nature. Swelling is the easiest ways to reduce pressure on printed materials. When combined with cellulose conversion reactions and stimuli such as water, it can

* Corresponding author.
E-mail address: bioladapo@abuad.edu.ng (B.I. Oladapo).

Peer review under responsibility of King Saud University.

Production and hosting by Elsevier

https://doi.org/10.1016/j.jksues.2019.12.002
1018-3639/

stimulate the time-based changes of 3D models to create 4-dimensional printing structures. This method is like the concept developed in "4D printing" and is used in MIT using small material shapes and volume expansion properties for performance response (Hashem et al., 2013; Hu et al., 2017). To obtain a cellulose fabric line to control the swelling of the matrix ends, 3D printing should be as transparent as previously described (Hashem et al., 2013). The present invention is generally used in the construction of ceramic commercial filament polymers of 3D systems used in laser printing, but also consisting of material pumps, which are a conventionally biodegradable and low cost (Borůvková, 2012; Adeoye et al., 2017). The invention is similar to filler is present in the PLA matrix polymer recycling plastic (polyol acid), but this method is limited. Concentrations of 1 to 4% should be printed in 3D (Ramanathan and Liu, 2005; Manu 2018; Oladapo et al., 2015; Ijagbemi et al., 2016). Organic paint composites are prepared by the dispersion of dispersed nanofibrils in alginate-based hydrogels of 95% of water crosslinked by immersion in $CaCl_2$ calcium chloride solution (Leigh et al., 2014). However, the number of biomaterials reported that cellulose manure is straightforward of 1.5 to 2.3%. Similar, similar bio-dry ink reported 3D printing obtained by lyophilisation of the biological representation of ink by the same method of printing with cellulose was declared as part of the project by investigations. Join the cellulose world value chain design (Postiglione et al., 2015, Bankole et al., 2019) of nanoscale alginate hydrogels compatible with good textures for 3D printing Kemp's Mug ranges from 0.5% to 1.3% w/w. Also, cellulose ink is designed specifically for 3D printing, ensuring that the cellulose compounds produced can be widely developed and used in the 4D printing research (Murphy, 2014; Du et al., 2017; Oladapo et al., 2019). In this research, a cellulose hydrogel, stimulant-sensitive, biodegradable inks was microstructurally analyse. This composite ink has been shown for 3D printing and has stability, flow and swelling that can occur. To obtain the correct position of the cellulose dye material and water-touch activity, intricate working patterns were created using 3D printing and demonstrated the ability to use this colour to produce 4D structures. In this study, the memory of the thermoplastic form was used in the mixed sedimentation process to create an ultra-sonication polymer composite structure (Bodaghi et al., 2018; Balogun and Oladapo, 2016). It was programmed in various forms for tensile strength and compression to study local recovery properties of different stresses. The research gives quantitative insight into the properties of 4D printing materials with FDM and ultra-sonication polymer composite, forms of memory. Therefore, the aim of this study is a comparative analysis of the biotechnological methods that could be suitable for the construction of artificial oasis and experimental testing of the most suitable biotechnology for the surface and treatment. Also, the evaluation of the composite microstructure particle of CMC in 4D surface luminance structure and the profile structure was done. The coss-sectional views and surface roughness, waviness profile of the specimens are extracted and analysed, with the corresponding Gaussian filter for the accurate decomposition of particles was analysed. The nanoparticle characterisation of the thermoplastic form was used in the mixed sedimentation process to create a polymer composite structure when analysing.

2. Materials and methods

There are many polymers obtained from cellulose that can produce hydrogel (Zhu, 2012). The polymer derived from cellulose selected for this study shows that it is easy to hydrate and repairs it because it is a source of sodium carboxymethylcellulose CMC. The polar nature of the carboxylic group dissolves the CMC in the water, causing gel formation. Fig. 1a-c represent an original scale value of SEM ultra-sonication, surface view of Karhunen-Loeve (KL) transforms of the threshold −69.8 nm minimum and 39.1 nm are maximum and surface luminance Gaussian filter (Sealy, 2016; Francis and Jain, 2016Li et al., 2017; Afolabi et al., 2019). Fig. 1d-e describe the frequency spectrum with volume islands nanoparticle and furrows KL transformed evaluation. These polymers are widely used in the food industry, skincare and as drug modifiers/rheology exchangers and are biologically compatible. The cotton fibre coating, such as those used in the paper industry, is selected as a component of the cellulose fibres although the purity of the pulp supplied has not been evaluated.

The profile enhanced CMC of KL transformed has 6sec transformation sequence of time (T) at length 77.0 mm of point 96.7 nm of the simulated value at 133 nm scale. The number of motifs of the experimental value is 188 at a mean height of 12.0 nm, with a pitch value of 6.84 mm of particle means an area of 31.8 mm^2 having equivalent diameter for each particle at 5.46 mm. The nanoparticle maintains a roundness smoothness of 0.496 and means compactness of 0.695. The information concerning extract profile waviness has a filter setting of the Gaussian filter at a cut-off value of 2.50 mm nanoparticle. The frequency movement of the particle was set at a magnitude of −68.4dBc at a zero-degree angle of zero wavelength. Fig. 2 shows a 3D view of the surface of the KL transformation. The number of islands has 424points at a threshold of 34.6 nm particle projected mean area of 8.37 mm^2 having mean compactness of 0.573 at the mean volume of $2.8328*10^{14}nm^3$ of the mean area ratio of 123 nm/mm^2.

All materials are used as planned. The planetary cutting machine is used to mix the ingredients. Carefully mixed mixtures, water mixture and a small amount of CMC of 15–20% by weight of the whole 30 ml of water were added, combined and 1600 rpm for 30 s before adding new minutes depending on the amount required. A clay of 0.5% montmorillonite by weight of water as a filler to steady the hydrogel. Montmorillonite platelets are rubbed in water with the appropriate mixture (Zheng et al., 2015). Inversion tests evaluated the evaluation of the stability of the gel formulas and the compounds containing CMC and soil for one-week samples in polypropylene bottles of 28micrometer in diameter and 115micrometer in length. The cellulose hydrogel compounds are compressed by hand with a 1 mm full syringe (as in a 3D print head) and dried to create a standard thin film. The CMC polymer is soaked in water. During the night to test the stability Automatic cross-linking cross-linking, polyacrylic acid (PCA) and citric acid (CA). It is related to the reactions of cross-linking performed and evaluated as Suspension Water at night Reaction crosslinking of citric acid, AAP and used for automatic cross-linking at 180 °C and the use of AAP touching at 120 °C for 10 to 30 min at 140 °C for 30 min. The reaction was determined (Borůvková and Wiener, 2012) and modified for the synthesis of hydrogel compounds. To create a 3:1 wt ratio of the hydrogel, CMC-Na and hydroxyethyl cellulose are used and are used in stones, instead of cross-linking between molecules to stimulate.

As expected, the citric acid formula has a lower potential than the cross-linked sample. However, it is necessary to create a controlled swelling without causing the material to deteriorate. Also, having a crosslinking agent other than crosslinking may help to control the level of crosslinking that affects the expansion potential. The role of the pulp strip in reducing swelling of the gel matrix is also observed. This formula is expected to be stable during hydration and water deficiency, such as citric acid and the post-solder pulp fibres found in the bridge of the CMC cellulose formula. The amount of citric acid crosslinking used in this method is derived from previous studies in the literature and remains constant as there are no significant parameters within the scope of the study.

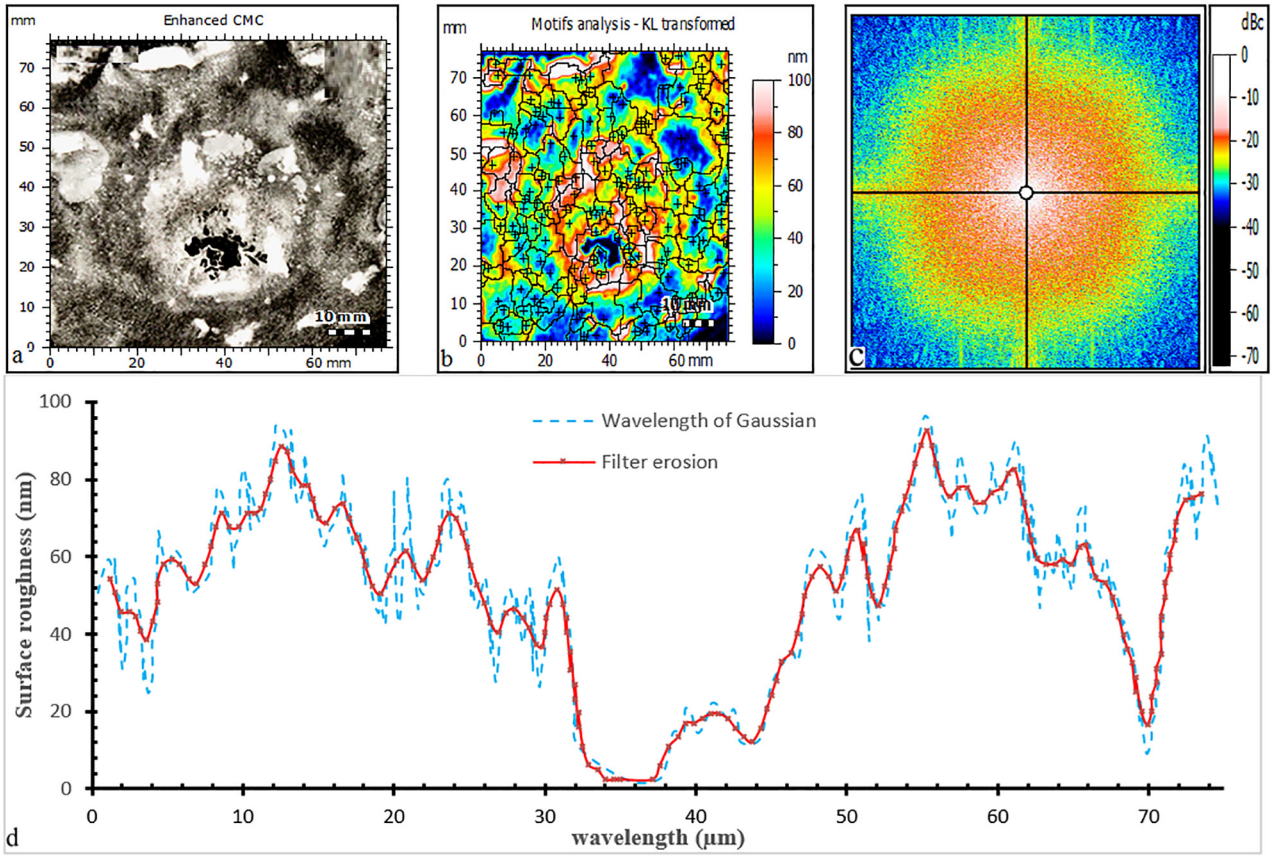

Fig. 1. Pulp-CMC composite films are illustrating enhancements in dispersion as a result of optimised fraternisation strategies ultra-sonication. (a) An original scale value of SEM ultra-sonication. (b) Motifs analysis of KL transformation. (c) **ultra-sonication** of CMC (d) Frequency spectrum.

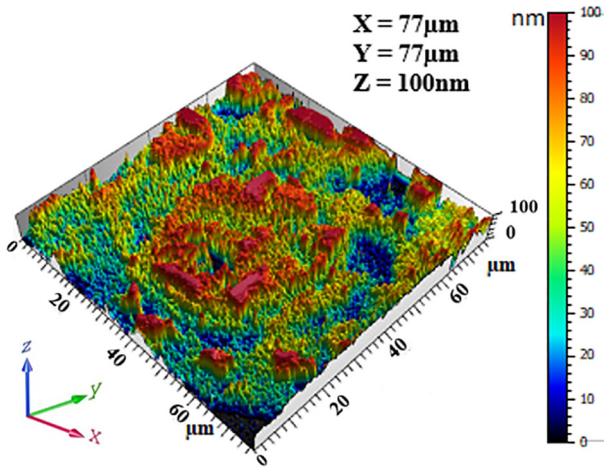

Fig. 2. 3D view of the surface of KL transformation of CMC.

3. Characterisation of inflammation rate.

The swelling response of the structural formula was studied by calculating the equilibrium ratio of the dry method and by immersion in water without anions by binding to the citric acid. It was placed and immersed in water without anions for 24 h to obtain stable swelling at room temperature 21 °C. The RS paper was calculated as follows:

$$y = 0.0038x^2 - 0.1105x + 24$$

$$Y = 33e^{2E\text{-}05x}$$

Where 'y' is the weight of the hydrogel/compound, and 'x' is the weight of the dry sample. The experiment to determine the swelling rate of the formulations also provides additional information on their aqueous stability.

3.1. 4D printing and rheological process

Scanning amplitude To determine the flow behaviour of hydrogels and compounds (deformation), frequency screening, static shear test and ramp test The gel sample shows sweep 0.01% to 100% voltage at a frequency of 1 Hz. Scan the rate of 0.1 Hz to 10 Hz in the gel sample at an energy of 0.5% in the linear viscoelastic movement system the geometry of the parallel layer 20 mm in diameter and all the samples examined at 25 °C. A samples 1.5 ml is used once, and the test tripled, and the error bar shows the corresponding standard deviation with a reasonable loading classification is used to assurance dependable and accurate installation protocols. The versatility of this method is the ratio of the number of crosslinking agents or cellulose polymers, which can be altered to obtain the specific increase required for the structure. The nanostructure surface change of ultra-sonication in time for 6 s on the simulation under the influence of temperature of 240 °C is shown in Fig. 3.

The process for preparing and processing competitive cellulose hydrogel formulas is summarised in Fig. 1 to create a balance between the advantages of fibre with no co-operation with the nature of the gel. Volume (Vf) 50% is selected from the final compound (Clower et al., 2017). Paper lens saturated with water for about 24 h. Fig. 3 shows a broad spectrum diagram of composite preparation. Also, there are many types of blending strategies ranging

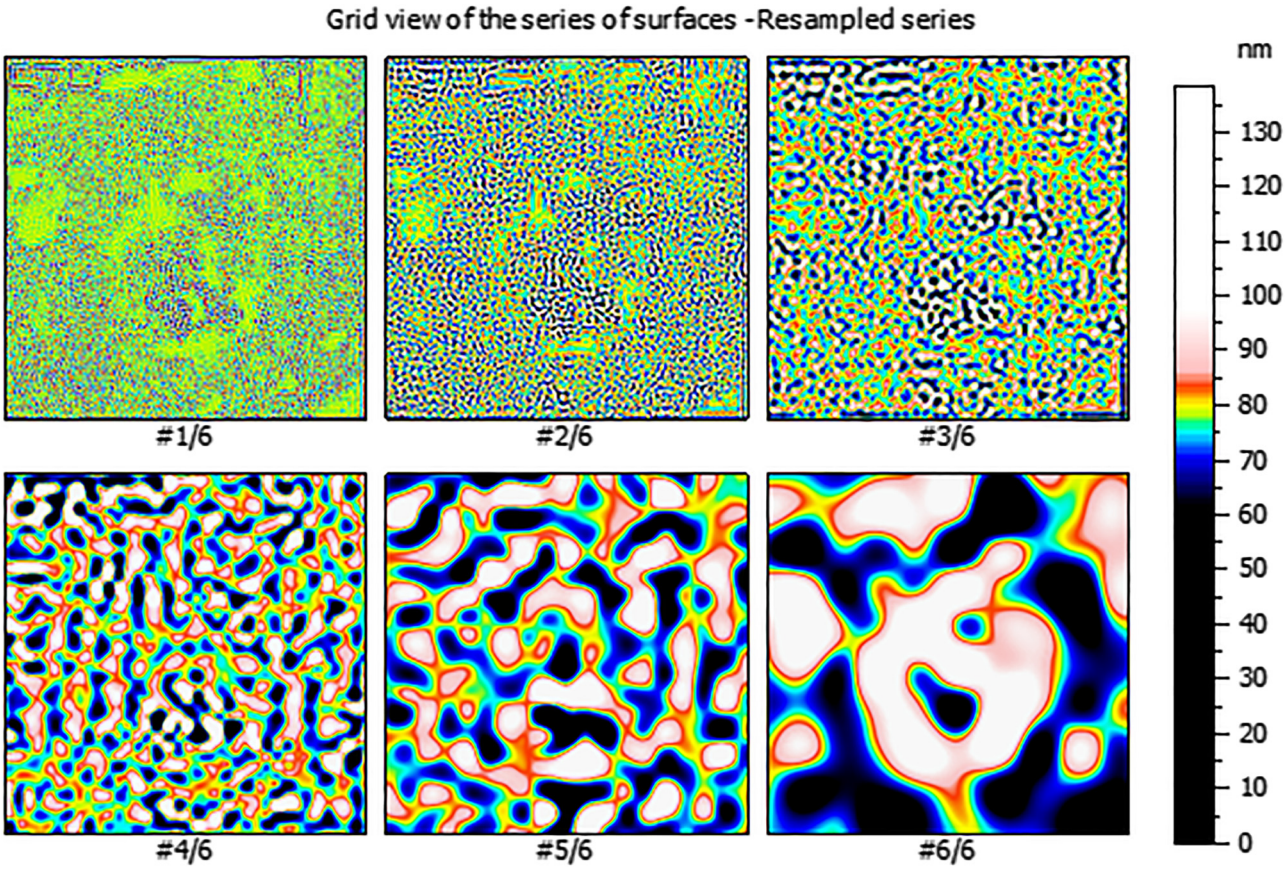

Fig. 3. The nanostructure grid series surface change of ultra-sonication under the influence of printing temperature of 6 s.

from sonication to shear mix to spatula in mechanical mixing. However, the composite received the results of the experiment below the ideal, as can be seen from the integration of the fibres observed in the film (Zuidema et al., 2014). However, it shows that during the extrusion process to increase hydrocolloid to CMC before and during the mixing of pulp in the water Fig. 4 shows that there are not many fibre groups for this formula distribution results. This is for high transparency in prepared films low; composite materials are derived from planetary mixers that use "rotating" movements and "Cycle" to ensure transparency by identifying areas where a high content mixture of fibre mass separation and distribution facilities with the addition of a polymer gel. To make the roll forming when combining all the components depending on the total volume for 3–4 min to obtain a homogeneous mixture. Add the bottom row to ensure that the extrusion is smooth. For the use of mixed ink in 3D printing, the stability of the long-term structure of the gel is an essential factor.

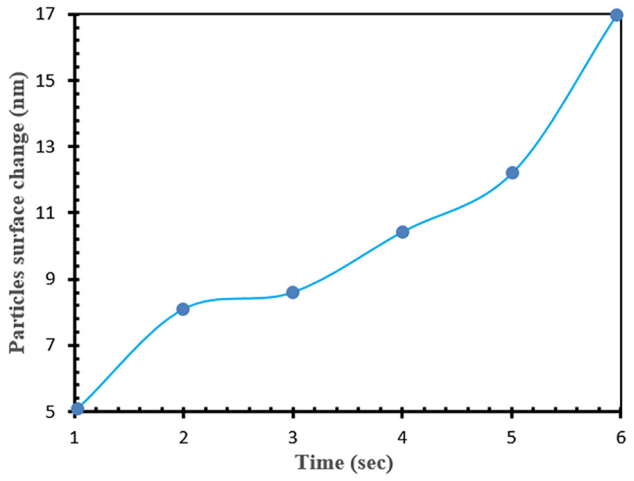

Fig. 4. 4D printing control chart that shows the optimal square of the six-point of surface change with time of ultra-sonication.

4. Results

Fig. 5 shows the elastic modulus G', and the phase angle (δ) as a purpose of the cut-off voltage of the sample analysed. The value of the missing module G" is not involved for clarity, but for the most applied stress regime, which indicates that G 45° is configured. The phase angle data is combined (δ) and phase angle data of modulus of elasticity measured in the linear viscoelastic system shows the maximum expected value for the Gel + Clay + CA is 1.15 kPa. The flexibility and viscosity are higher than the gel sample + CA (0.9 kPa), which is different from the gel sample. It should be considered that the data of δ for CA (low) will be noisy, especially at a voltage of 0.01% to 0.1% for reduction of response in this period. The control chart that shows the optimal square of the six-point of 4D printing production of the system is shown in Fig. 4.

The results showed that the change of G and the angle, the value of the modulus and the loss of G for the opening were neglected and that the relative importance of the modulus of elasticity and the viscosity modulus would be compared. With the phase-frequency angle of elastic modulus at 1 Hz, it corresponds to the G-value of the LVER format (Abuzaid et al., 2018; Damanpack et al., 2017). The recorded response indicates that the modulus depends on the speed and relaxation of the indicated blades from

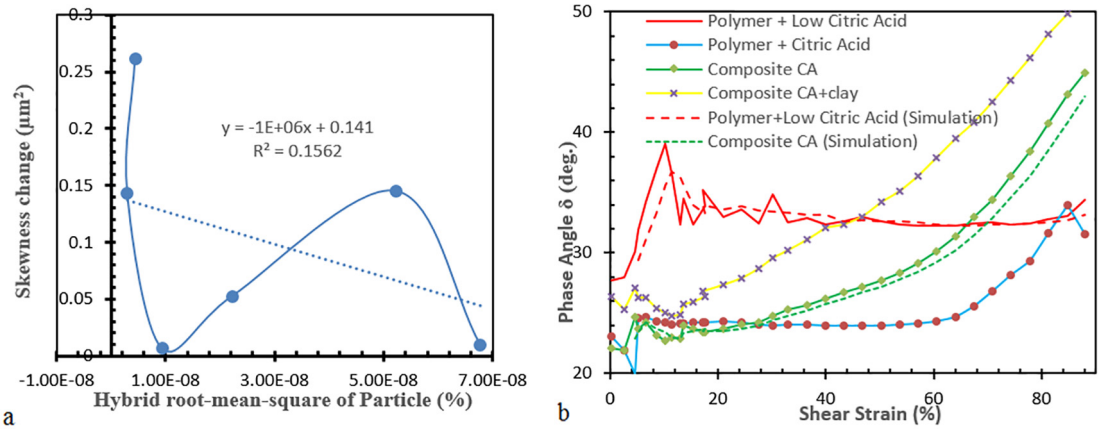

Fig. 5. (a) the six-point of the experimental value of the change in time of the hybrid sample (b) Amplitude sweep data are showing the elastic modulus (G′) (Log scale) and phase angle (δ) as the function of shear strain.

45 bar to 45°. Range The frequency determines the trend of the phase angle that represents the frequency. The frequency of the change is correct, and the time remaining is not complete because there is not enough time to explore the low-frequency levels. The amplitude is structured, as indicated in the analysis results.

The result of the static slip measurement shown in Fig. 6 is the shear rate and viscosity compared to the shear rate. The sample is hugely thinner by reducing the viscosity response rate, which confirms the expected artificial behaviour. Also, the relationship between shear stress and applied. Although the viscosity and pressure of the composite + soil + CA sample are twice as high as the solid in the example, it may be noted that there is a gel + CA sample that is narrower lower, especially at a high cut-rate. These results show that the composite system with excellent extrusion properties for homogeneous phase 3D printing does not affect the efficiency of the gel paste or strength, high above the solid who want to rest and is not reduced.

Performance limitations refer to the tension that is necessary to interfere with the physical response that provides the properties of the material, such as solids, material flow. In other words, if the stress that is applied exceeds the critical threshold value, commonly referred to as the yield strength of this material, the material will flow below this limit flow occurs about the system. The content described here means that when applied through the piston, the formula may be extruded from the cylinder. The printer Strain strain is one of the most commonly used test methods for stress assessment of physical fitness, which measures the instant viscosity of the sample compared to the increase in shear strength. Shear stress of elastic limit that corresponds to the maximum thickness is estimated, such as stress, stress. Data of the viscosity of the ramp measured from the formula used to determine the stress ramp mean value and the flow resistance of the equation. Data collection is done three times and using examples. Each sample Only once the lifetime of the bar is maintained at 100 s for all formulas. However, it has been maintained with different final strength (zero) to capture the most significant viscosity changes and superior response performance

For example, Gel + Clay + CA were sent from 0 to 300 Pa, while Composite + CA and Compound + Clay + CA samples were sent at 0–200 Pa during the test. For clarity, the viscosity error bar was removed from Fig. 7 the sample gel + CA low was removed from the stress ramp test to evaluate the confrontation to flow. Although the low viscosity is suitable for extrusion throughout the syringe, the formula is careful too small in G to maintain the compression shape. The tensile strength for each method is derived from the cut resistance consistent to the supreme thickness for each test. It is presented in Fig. 7 the information accessible here is more dependable because it signifies the actual test data in the results shown in Fig. 6, including the maximum values shown in the graph. The gel + CA and the gel + Arca + California have the highest production stress affected by loading errors, making it difficult to get rid of the syringe compared to other low weight formulas.

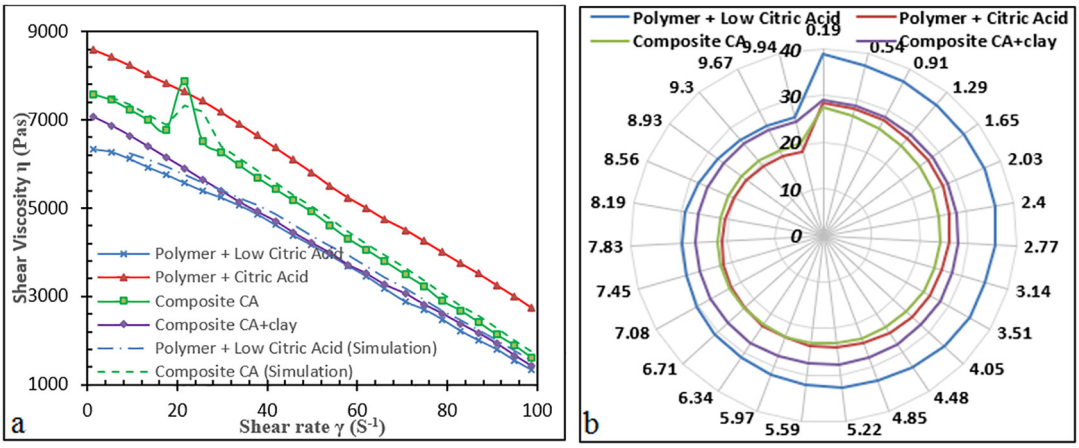

Fig. 6. Polar Steady-state shear viscosity (η) (Log scale) and shear stress (τ) as a function of shear rates (b) Frequency sweep data are showing the elastic modulus (G′) (Log scale) and phase angle (δ) as a function of frequency.

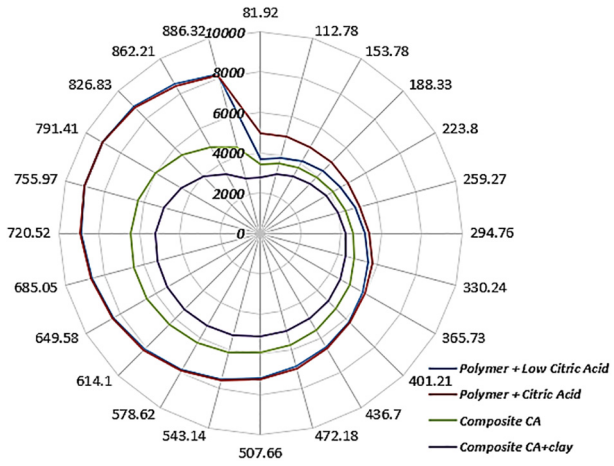

Fig. 7. Polar Stress ramp plots yield stress of formulations at peak viscosity.

According to the sum of clay and fibre pulp, it helps clean the flow of the value of the return boundary. The representation of 3D printing of cellulose compounds containing the delicate production and presentation of the flower petals architecture is shown in Fig. 7. This new configuration was created by the more significant deformation differences obtained from the check. Dehydration of materials at high temperatures converted form is embedded by placing it in a water bath at room temperature in a straightway. Similarly, we can expect the efficiency of the cellulose cycle at Printed in 3D but can be scheduled at a reduced rate because the matrix supports hydrogels that adapt to changes in shape. Consolidated fibres example is shown in Fig. 7, not only demonstrates the ability of the material system developed for 3D printing but can also reduce plane levels due to the turbulence of dehydration/moisture programs. The resulting compounds are created to have 50% fibre by weight and 50% CMC, which results in higher fibre content.

5. Conclusions

In conclusion, the evaluation of the composite microstructure particle of CMC in 4D surface luminance structure and the profile structure was done. Cross-sectional views and surface roughness, waviness profile of the specimens are extracted and analysed, with the corresponding Gaussian filter for the accurate decomposition of particles was carried out. The nanoparticle characterisation of the thermoplastic form was used in the mixed sedimentation process to create a polymer composite structure when analysing. The fact that the tissues of the pulp are not only separated by hydrogels but also provides the required roughing properties also helps to divide and distribute the pulp fibres with the optimal mixing strategy. Also, it is observed that there is a moderate reaction to the high content of anhydride in citric acid during the dehydration, which indicates that interdependent substances interact with cellulose. However, it was observed that the leakage potential of the components particles after hydration and dehydration have an effect on shape memory. The uniform distribution of composite biomaterials and components in the pulp network prevent clay particles composition from escaping from the crosslinked samples.

Declaration of Competing Interest

The authors declare that they have no known competing financial interests or personal relationships that could have appeared to influence the work reported in this paper.

Acknowledgement

This project is funded by the Higher Education Innovation Fund (HEIF) of De Montfort University 2018–2019, UK: Research Project No. 0043.06.

References

Adeoye, A.O.M., Joseph, F.K., Bankole, I.O., Samuel, O.A., 2017. Experimental analysis and optimisation of synthesised magnetic nanoparticles coated with PMAMPC-MNPs for bioengineering application. St. Petersburg Polytechn. Univ. J. Phys. Math. 3 (4), 333–338.

Afolabi, S.O., Oladapo, B.I., Adeoye, A.O.M., Kayode, J.F., 2019. Design and finite element analysis of a fatigue lifeprediction for safe and economical machine shaft. Journal of Materials Research and Technology 8 (1), 105–111. https://doi.org/10.1016/j.jmrt.2017.10.007.

Almeida, Ana P.C., Conejo, João P., Fernandes, Susete N., Echeverria, Coro, Almeida, Pedro L., Godinho, Maria H., 2018. Cellulose-based biomimetics and their applications. Adv. Mater. 30 (19), 1703655.

Bakarich, S.E., Spinks, G.M., 2015. 4D printing with mechanically robust, thermally actuating hydrogels. MRC 36, 1211–1217.

Oladapo, Bankole I., Adeoye, Adeyinka O.M., Ismail, Muhammad, 2018a. Analytical optimisation of a nanoparticle of microstructural fused deposition of resins for additive manufacturing. Comp. Part B: Eng. 150, 248–254.

Oladapo, B.I., Vincent, B.A., Oke, A.O., Agbor, E.A., 2015. Design and finite element analysis on car seat height screw adjuster using autodesk inventor. Int J Sci Res Eng Stud (IJSRES) 2 (8).

Oladapo, Bankole I., Zahedi, S.A., Adeoye, A.O.M., 2019. 3D printing of bone scaffolds with hybrid biomaterials. Compos. Part B: Eng. 158, 428–436.

Oladapo, Bankole I., Abolfazl Zahedi, S., Vahidnia, F., Ikumapayi, O.M., Farooq, Muhammad U., 2018b. Three-dimensional finite element analysis of a porcelain crowned tooth. Beni-Suef Univ. J. Basic Appl. Sci. 7 (4), 461–464.

Bodaghi, M. Damanpack A. R. and W H Liao, Triple shape memory polymers by 4D printing, Published 8 May 2018 • © 2018 IOP Publishing Ltd, Smart Materials and Structures, Volume 27, Number 6.

Damanpack, M., Bodaghi, A.R., Hu, G.F., Liao, W.H., 2017. Large deformations of soft metamaterials fabricated by 3D printing. Mater. Design 131, 81–91.

Borůvková K. Thermal self cross- CMC, ACC. J. XVII (2012) 6-13.

Borůvková, K. J. Wiener, S. Kukreja, Thermal self cross-linking of carboxymethylcellulose, Acad. Coord. Cent. J. XVII (2012) 6 13.

Balogun, V.A., Oladapo, B.I., 2016. Electrical energy demand modeling of 3D printing technology for sustainable manufacture. International Journal of Engineering 29 (7), 954–961.

Bankole, I.O., Zahedi, S.A., Chong, S., Omigbodun, F.T., Malachi, I.O., 2019. 3D printing of surface characterisation and finite element analysis improvement of PEEK-HAP-GO in bone implant. The International Journal of Advanced Manufacturing Technology, 1–13.

Chang, C.L., 2011. Zhang, Cellulose-based hydrogels: present status and application prospects. Carbohydr. Polym. 84, 40–53. https://doi.org/10.1016/j.carbpol.2010.12.023.

Demitri, C., Nicolais, L., 2008. Novel superabsorbent cellulose-based hydrogels with citric acid. J. Appl. Polym. Sci. 110, 2453–2460.

Du, H., Liu, L., Zhang, F., Zhao, W., Leng, J., Liu, Y., 2017. Thermal-mechanical behaviour of styrene-based shape memory polymer tubes. Polym Testing 57, 119–125.

Francis, V., Jain, P.K., 2016. Experimental investigations on fused deposition modelling of polymer-layered silicate nanocomposite. Virtual Phys. Prototyp. 11, 109–121.

Håkansson, K.M.O., Gatenholm, P., 2016. Solidification of 3D printed nanofibril hydrogels into functional 3D cellulose structures. AMP 1.

Hashem, S., Sharaf, M.M. Abd, El-Hady, A. Hebeish, 2013. Synthesis and characterisation of novel CMC hydrogels and CMC-hydrogel- ZnO-nanocomposites. Carbohydr. Polym. 95, 421–427.

Hu, G F. Damanpack, A R., Bodaghi M., Liao, W. H. Increasing dimension of structures by 4D printing shape memory polymers via fused deposition modelling, Published 10 November 2017 • © 2017 IOP Publishing Ltd, Smart Materials and Structures, Volume 26, Number 12.

Ijagbemi, C.O., Oladapo, B.I., Campbell, H.M., Ijagbemi, C.O., 2016. Design and simulation of fatigue analysis for a vehicle suspension system (VSS) and its effect on global warming. Procedia engineering 159, 124–132.

Leigh, C.P., Purssell, D.R., Billson, D.A., 2014. Hutchins, Using magnetite/thermoplastic composite in 3D printing of direct replacements for commercially available flow sensors. Smart Mater. Struct. 23, 095039.

Li, S.S., Zahedi, S.A., Silberschmidt, V., 2017. Numerical Simulation of Bone Cutting: Hybrid SPH-FE Approach. Numerical Methods and Advanced Simulation in Biomechanics and Biological Processes, 187–201.

Manu, C., 2018. Responsive cellulose-hydrogel composite ink for 4D printing. Mater. Design 160, 108–118.

Murphy, A Atala, 2014. 3D bioprinting of tissues and organs. Nat. Biotechnol. 32, 773–785.

Oladapo, B.I., Zahedi, S.A., Omigbodun, F.T., Oshin, E.A., Adebiyi, V.A., Malachi, O.B., 2019. Microstructural evaluation of aluminium alloy A365 T6 in machining operation. J Mater Res Technol 8 (3), 3213–3222.

Postiglione, G., Natale, G., Gryphon, M., Levi, S., 2015. Turri, Conductive 3Dmicrostructures by direct 3D printing of polymer/carbon nanotube nanocomposites via liquid deposition modelling. Compos. Part A: Appl. Sci. Manuf. 76, 110–114.

Ramanathan, H., Liu, L.C., 2005. Brinson, Functionalized property improvement. J. Polym. Sci. Part B: Polym. Phys. 43, 2269–2279.

Sealy, C., 2016. 3D printing makes bone scaffolds a better fit. Mater. Today 19, 557.

Abuzaid, Wael, Alkhader, Maen, Omari, Mohamed, 2018. Experimental analysis of heterogeneous shape recovery in 4d printed honeycomb structures. Polymer Testing 68, 100–109.

Clower, William, Groden, Nicholas, Wilson, Chester G., 2017. Graphene nanoscrolls fabricated by ultrasonication of electrochemically exfoliated graphene. Nano-Struct. Nano-Objects 12, 77–83.

Li, Xin, 2017. Intelligent materials: a review of applications in 4D printing. Assembly Automation 37 (2), 170–185.

Zheng, W.J., 2015. Facile fabrication of self-healing CMC hydrogels. Eur. Polym. J. 72, 514–522.

Zheng, J., Gao, Z., Wei, J., Zhou, Y.M Chen, 2015. Facile fabrication of self-healing carboxymethyl cellulose hydrogels. Eur. Polym. J. 72, 514–522. https://doi.org/10.1016/j.eurpolymj.2015.06.013.

Zhu, Y., 2012. Rapidly switchable shape-memory elastomer nanocomposites. Soft Mater. 8, 2509–2517.

Zuidema, C.J., Rivet, R.J., Gilbert, F.A., 2014. Morrison, A protocol for rheological characof hydrogels for TE strategies. J. Biomed. Mater. Res. B Appl. Biomater. 102, 1063–1073. https://doi.org/10.1002/jbm.b.33088.